



This is a repository copy of *Computationally Efficient 3D Eddy Current Loss Prediction in Magnets of Interior Permanent Magnet Machines*.

White Rose Research Online URL for this paper:
<http://eprints.whiterose.ac.uk/100922/>

Version: Accepted Version

Article:

Nair, S.S., Wang, J. orcid.org/0000-0003-4870-3744, Chen, L. et al. (3 more authors)
(2016) Computationally Efficient 3D Eddy Current Loss Prediction in Magnets of Interior Permanent Magnet Machines. *IEEE Transactions on Magnetics*, 52 (10). 8108110. ISSN 0018-9464

<https://doi.org/10.1109/TMAG.2016.2582145>

© 2016 IEEE. Personal use of this material is permitted. Permission from IEEE must be obtained for all other users, including reprinting/ republishing this material for advertising or promotional purposes, creating new collective works for resale or redistribution to servers or lists, or reuse of any copyrighted components of this work in other works.

Reuse

Unless indicated otherwise, fulltext items are protected by copyright with all rights reserved. The copyright exception in section 29 of the Copyright, Designs and Patents Act 1988 allows the making of a single copy solely for the purpose of non-commercial research or private study within the limits of fair dealing. The publisher or other rights-holder may allow further reproduction and re-use of this version - refer to the White Rose Research Online record for this item. Where records identify the publisher as the copyright holder, users can verify any specific terms of use on the publisher's website.

Takedown

If you consider content in White Rose Research Online to be in breach of UK law, please notify us by emailing eprints@whiterose.ac.uk including the URL of the record and the reason for the withdrawal request.



eprints@whiterose.ac.uk
<https://eprints.whiterose.ac.uk/>

Computationally Efficient 3D Eddy Current Loss Prediction in Magnets of Interior Permanent Magnet Machines

Sreeju. S. Nair*, Student Member IEEE, Jiabin Wang*, Senior Member, IEEE, Liang Chen*, R. Chin †, I. Manolas†, and D. Svehkarenko†

*Department of Electronic and Electrical Engineering, The University of Sheffield, Sheffield, S1 3JD, United Kingdom

†ABB Corporate Research, SE-721 78 Västerås, Sweden

Abstract -- This paper proposes a computationally efficient method based on imaging technique, for accurate prediction of 3-dimensional (3D) eddy current loss in the rotor magnets of interior permanent magnet (IPM) machines. 2D time-stepped finite element analysis is employed to generate the radial and the tangential 2D magnetic field information within the magnet for application of the 3D imaging technique. The method is validated with 3D time-stepped finite element analysis (FEA) for an 8 pole-18 slot IPM machine evaluating its resistance limited magnet loss with increase in axial and tangential segmentation. Magnet loss considering eddy current reaction at high frequencies is evaluated from the proposed method by employing the diffusion of the 2D magnetic field variation along the axial plane. The loss associated with all the frequencies together in the armature currents is evaluated by considering each of the harmonics separately in the proposed method employing the frozen permeability to account for magnetic saturation. The results obtained are verified with 3D FEA evaluating the magnet loss at fundamental, 10 and 20 kHz time harmonics in armature currents.

Index Terms— Eddy current loss, finite element, frozen permeability, imaging method, permanent magnets.

I. INTRODUCTION

High power density IPM machines are increasingly being used in a variety of applications, including high speed manufacturing [1], power generation [2], hybrid and electric tractions [3-6], aerospace [7] and ship propulsion [8]. These machines can be operated over a broad range of speeds when compared to surface mounted permanent magnet (SPM) machines by employing flux weakening control [9-11].

On the other hand, at higher speeds IPM machines especially with concentrated windings, produce increased electromagnetic filed variations which are associated with space harmonics from stator winding distribution in addition to slotting and also time harmonics from the armature currents [12-15]. While the pole shoes may prevent these harmonics from penetrating in to the magnets, the presence of flux barriers and the saturations of the silicon steel laminations will allow them eventually entering the magnets and cause eddy current loss. The loss in the magnets can raise their operating temperature and hence the knee point flux density of the magnets, thus making them more vulnerable to partial demagnetization in an event of sudden short circuit [16], [17]. An accurate estimation of magnet loss enables to reduce the loss at the design stage of the machine by devising necessary changes in the geometry and also by implementing feasible axial / tangential segmentations.

The highly nonlinear nature of the rotor core and the complicated boundary conditions makes a complete analytical estimation of the magnet loss almost impossible in IPM machines. However a few analytical insight can be derived on the magnet loss based on which the design parameters can be altered for reducing them [18]. The much simplified theoretical estimation of magnet loss proposed to evaluate the eddy currents associated with carrier harmonics in IPM machines approximates an uniform source field along the magnets [19],[20]. Also another simplified analytical estimation of permanent magnet loss proposed in [21-23], ignores the saturation effects of silicon steel laminations and neglects any filed variation along its radial direction. This approximation

deviates from the real flux density distribution in magnets significantly and results in poor accuracy in loss estimation. Hence numerical analysis becomes indispensable in accurately estimating the loss in the permanent magnets for such machines.

2D time-stepped finite element analysis (FEA) gives fairly good results in eddy current loss evaluation, however its accuracy is compromised if the axial length of magnets is comparable to their other dimensions since the eddy current flow in the magnets may become predominantly 3-dimensional (3D) with reduced axial lengths. The highly accurate 3D FEA for IPM machines [13], [24] is rather time consuming and requires immense memory in storing the results. There are a few reduced order 2D-3D numerical methods proposed to overcome the computational burden involved in direct 3D finite element calculations [25-27]. The method in [26] evaluates the magnet loss at each frequency of interest in 3D FEA by employing differential permeability derived from 2D FEA calculations. Whereas the method proposed in [27] models only the permanent magnet in 3D FEA and inputs the magneto-static field obtained from 2D FEA for loss evaluation. Although these methods may be computationally efficient, they have a varying degree of accuracy. Magnet loss evaluation at each frequency of concern separately considering average differential permeability, may also fail to consider the effective magnetic saturation of the silicon steel laminations arising out of all the armature harmonics in the machine. To elude the computational burden of 3D FEA completely in PM loss evaluation, the method proposed in [28] predicts the resistance-limited eddy current loss analytically from the magnetic field derived from few magneto-static computations. This method approximates the 3D end effects of eddy currents by considering rectangular loops of varying perimeter along the axial plane, and hence predicts the eddy current distribution within the magnets at reduced accuracy. Moreover, it fails to assess the contribution of magnet loss associated with the tangential component of the magnetic field.

The method of generalized imaging is proposed in [29] to

evaluate the resistance limited eddy current distribution which satisfies its natural boundary condition for the magnets in a SPM machine neglecting any curvature effects. The method establishes the distribution of magnetic field variation with time as the sources of the eddy current fields in the form of 3D Fourier series in x, y, z directions. Ultimately only the coefficients for the sines and cosines needed to be evaluated in loss computation using Fourier expansion in three dimensions. However, the 3D eddy current source distribution applied here does not include the eddy current reaction effect which may be significant at high frequencies.

This paper proposes a computationally efficient method based on the imaging technique, for accurate prediction of 3-dimensional (3D) eddy current loss in the rotor magnets of IPM machines. The magnetic field variation with time as the source of the eddy current field is obtained from 2D FE, and the axial field variation at high frequencies due to eddy current reaction is incorporated in the 2D FE results based on the solution to 2-D diffusion equation before being applied in the imaging method. Finally, the combined loss evaluation associated with fundamental and the carrier frequency harmonics in the armature currents is evaluated by employing the frozen permeability concept to account for the stator and rotor iron core saturation. The method is validated with 3D time-stepped finite element analysis (FEA) on an 8-pole, 18-slot IPM machine.

II. IMPLEMENTATION OF PROPOSED METHOD FOR IPM MACHINES

A. Machine Topology and Design Parameters

The analytical part of the imaging method for predicting resistance limited 3D eddy current distribution and the total eddy current loss has been presented in [29]. Without loss of generality, the imaging method is implemented on the 8-pole, 18-slot IPM machine [30] employing V shaped NdFeB magnets with its cross section as shown in Fig.1. The machine topology benefits from low-space harmonics [31] and, hence, low eddy current loss, improved reluctance torque and less demagnetization risk. The machine is designed for EV traction applications and has been optimized for maximum energy efficiency over the combined drive cycles of the New European Driving cycle (NEDC) and the Artemis Urban Driving Cycle (Artemis) while satisfying the machine torque, speed specifications as well as volumetric, electrical, thermal and mechanical design limits [32-34]. The key specifications and geometric parameters of the machine are listed in Table 1. For the analysis, the rotor position is defined as 0° when the center of magnet '1' and magnet '2' is aligned horizontally, as shown in Fig.1.

B. Extraction of Field Information from 2D FEA

To implement loss evaluation in the proposed method, the flux density values need to be captured to form a matrix. Unlike the case with SPM machines where the magnet field orientations are referred w.r.t the global $r-\theta$ co-ordinate system, the orientation of field associated with each magnet is different for the case with IPM machines. Hence the values in each matrix should correspond to the source at a location given by the local

$x-y$ coordinates attached separately to every magnet. Thus the magnetic flux density values from the 2D FEA are extracted using a mesh grid constructed over the magnets as shown in Fig.2. Considering the machine symmetry, only one half of the machine needs to be modelled in loss evaluation and hence mesh grids are constructed only over the eight magnets. Every point of intersection on this mesh forms the x and y coordinates of the field information. For the machine under consideration without any segmentation in the x -direction, each magnet as shown in Fig.2 (a) is discretized into thirty-two divisions along the x and y directions. The number of divisions within a magnet segment may be modified according to the number of tangential (in the x direction) segmentations. For example, the mesh is modified as shown in Fig.2 (b) with sixteen divisions along the x directions in the analysis for the case with two tangential segmentations.

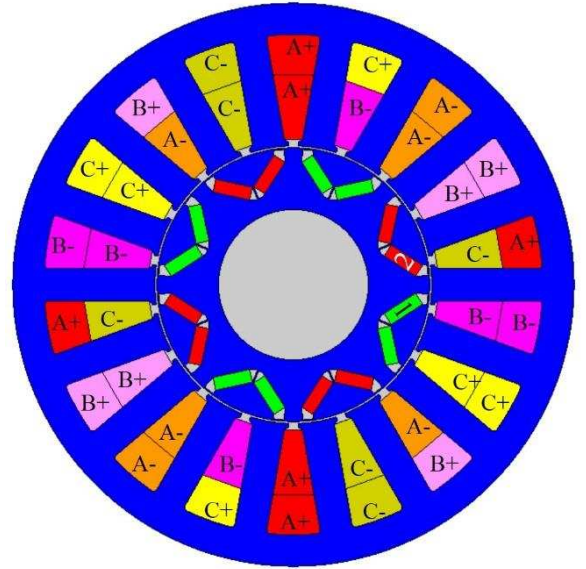


Fig.1. Cross sectional schematic of 8-pole,18-slot IPM machine.

TABLE I
IPM SPECIFICATIONS AND KEY DIMENSIONS

Parameter	Unit	Value
Base speed	rpm	1350
Maximum Speed	rpm	4500
Peak torque below and at base speed	Nm	70
Continuous torque below and at base speed	Nm	35.5
Maximum Current Limit	A	170
Nominal DC link voltage	V	120
Stator outside diameter	mm	150
Stator bore diameter	mm	73.9
Rotor outside diameter	mm	72.9
Magnet width	mm	3.5
Magnet length	mm	10
Stack length	mm	118
Slot opening	mm	2.5
Shaft diameter	mm	40
Magnet Resistivity	$\Omega.m$	1.8×10^{-6}

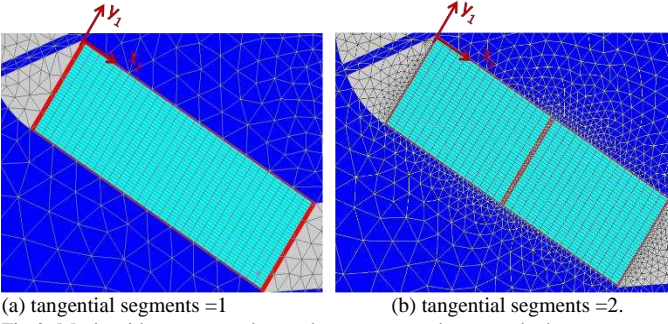


Fig.2. Mesh grids constructed over the magnets and are attached to separate coordinate system at $\omega t = 0$ position.

C. Implementation of 2D FEA Results in the Proposed Method.

However, since the flux density values (B_{x_1}, B_{y_1}) captured are referred in the stationary (x_1, y_1) coordinates attached to the magnets at the initial rotor position, the values needed to be transformed to the co-ordinate system which rotates with the magnets as shown in Fig.3. This ensures the eddy current sources [29] ($S_{x_1} = \partial B_{x_1} / \partial t, S_{y_1} = \partial B_{y_1} / \partial t$) seen by the magnets are referred in the rotor coordinate system. Hence the flux density values ($B_{x_{r1}}, B_{y_{r1}}$) at an angular position ωt w.r.t the rotating co-ordinate system (x_{r1}, y_{r1}) attached to the magnets at time t can be calculated as,

$$B_{x_{r1}} = B_{x_1} \cos(\omega t) - B_{y_1} \sin(\omega t) \quad (1)$$

$$B_{y_{r1}} = B_{x_1} \sin(\omega t) + B_{y_1} \cos(\omega t) \quad (2)$$

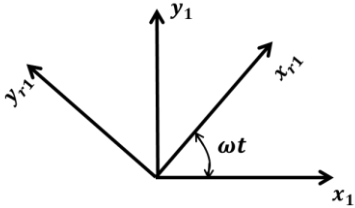


Fig.3. Rotor coordinate system (x_{r1}, y_{r1}) displaced at an angle ωt w.r.t the stationary system (x_1, y_1).

The eddy current sources ($S_x = \partial B_x / \partial t, S_y = \partial B_y / \partial t$) are evaluated from flux density values obtained from two consecutive time intervals. The source values are discretized together with their images in three dimensions in each magnet bounded by ($2L_x, 2L_y, 2L_z$). The number of discretization in the z -direction should be sufficiently large to ensure high accuracy. For the machine under consideration 32 divisions are considered for the unsegmented magnet length (L_z) along the axial direction. 3D FFT is performed to evaluate the source coefficients and hence the eddy current density coefficients [29]. The eddy current loss in every magnet is calculated at each time step and the analysis are repeated for $1/6^{\text{th}}$ electrical cycle to predict the average loss.

To evaluate the loss variations with number of axial and tangential segmentations of the magnet, the losses are evaluated for each tangential segment separately and the total magnet loss is computed as the sum of these losses multiplied with the

number of axial segments for the IPM machine. The loss in each axial segment is considered identical as the source field is treated essentially 2D and hence no variation along the axial direction. For example, for the machine having n_c tangential segments and n_a axial segments in a magnet as shown in Fig.4, eddy current loss is evaluated for each tangential segment separately employing its dimensions (L_{xs}, L_y, L_{zs}) in the imaging method [29]. The total loss per magnet is evaluated as the sum of the loss from the n_c tangential segments multiplied with the number of axial segmentation n_a . This way of evaluation quantifies the loss in each magnet segment, which will enable the designer to optimize the number of magnet segments, and hence to control the loss distribution among them.

Since the calculations are performed in 3-dimensional space for each harmonic, matrix operations are used to facilitate efficient calculations. The entire process is implemented in Matlab, and it takes around 60 minutes to generate the flux density harmonics from 2D FEA and less than 30 seconds to compute the total 3D eddy current loss for all the magnets in a typical PC. Hence on an average for evaluating the loss variation with increase in axial number of segmentation up to 12, it takes around 5 minutes for each case. In contrast, it takes more than 7 days for one 3D FE analysis with no axial segmentation on a typical 3.3 GHz, 64GB PC.

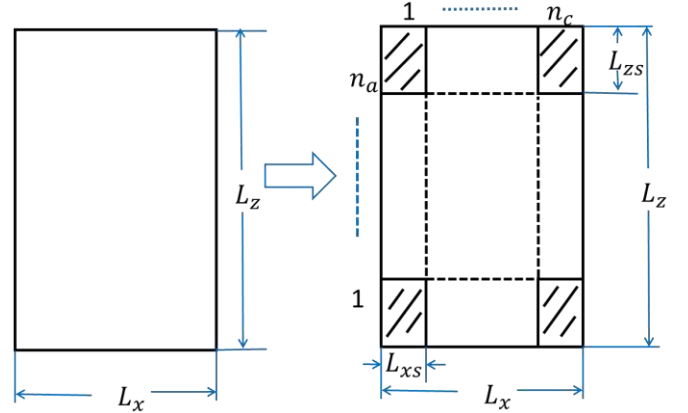


Fig.4. Segmentation of the magnet in axial and tangential direction.

III. 3D FINITE ELEMENT VALIDATION

A 3D FE model of the machine as shown in Fig.5 has been built to predict the 3D eddy current distribution and resultant eddy current loss induced in the magnets. Since the machine employs fractional slot per pole topology, circumferential symmetry exists only over 180 mechanical degrees. Thus, a quarter of the machine has to be modelled in 3D FEAs. Tangential magnetic field boundary condition is imposed on the circumferential surface. The meshed coils are extended in axial directions to consider the end effect. Tangential boundary conditions are imposed on this extended surface. In addition, perfect insulation boundaries are applied to the end surfaces of the magnets.

Magnet loss are evaluated at the maximum speed of the machine ($N = 4500 \text{ rpm}$), when the armature current is 61.17(RMS), having a flux weakening angle $\gamma = 73.27^\circ$.

Under such operating conditions the effect of eddy current reaction is negligible and hence the magnet loss is considered resistance limited. This is because the skin depth evaluated at this operating frequency is comparable with magnet dimensions. The predicted loss variations by the 3D imaging method, 3D FE and 2D FE with number of axial and tangential segments at the peak load conditions are compared in Fig.6 and Fig.7. It can be observed that the magnet loss evaluated from the 3D imaging method matches very well with the 3D FEA results, while significant error occurs with 2D FEA with increase in the number of axial segmentations.

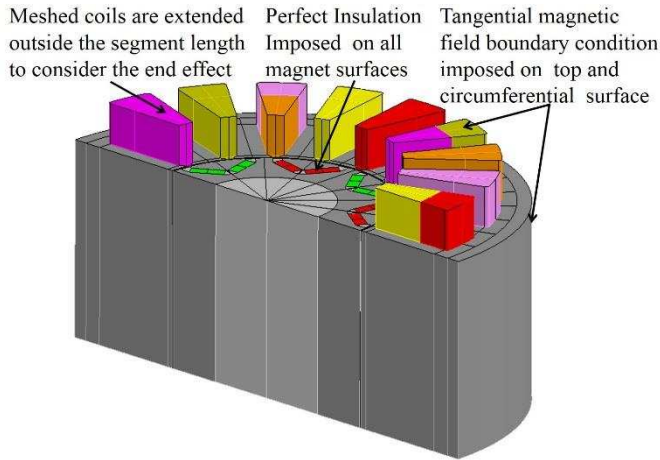


Fig.5. 3D FE model based on symmetry

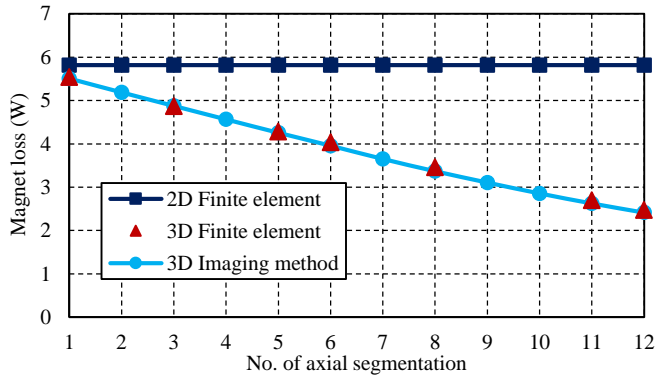


Fig.6. Comparison of eddy current loss variations with axial number of segments when the number of tangential segments = 1

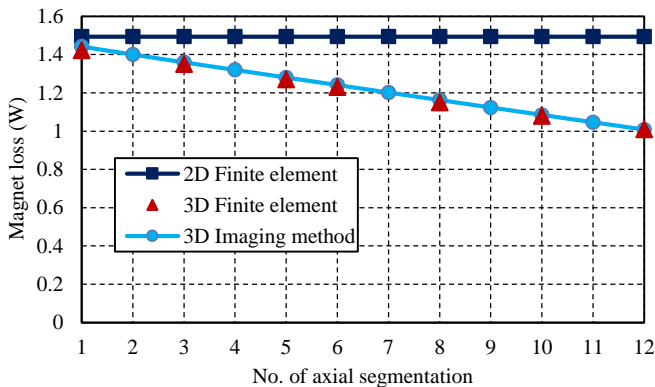


Fig.7. Comparison of eddy current loss variations with axial number of segments when the number of circumferential segments = 2.

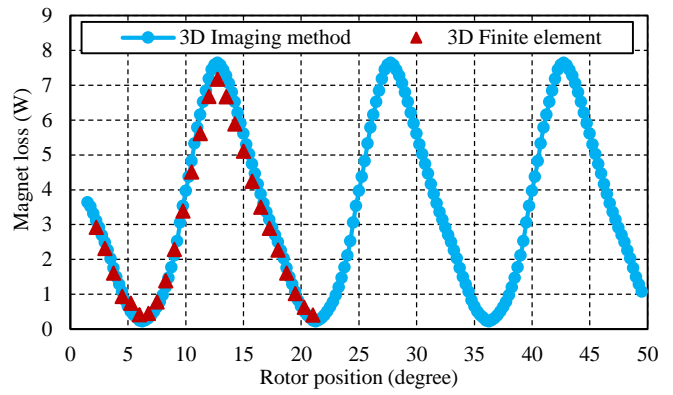


Fig.8. Comparison of instantaneous loss variation from imaging method and 3D FEA.

The instantaneous variations of the total magnet loss with rotor position predicted by the imaging method and by 3D FEA are compared in Fig.8. It is clear from the figure that the loss predicted by the imaging method follows very well with the 3D FEA results. The slight difference from the 3D FE simulation with the imaging method may be attributed to the winding end effect which is neglected in the imaging method.

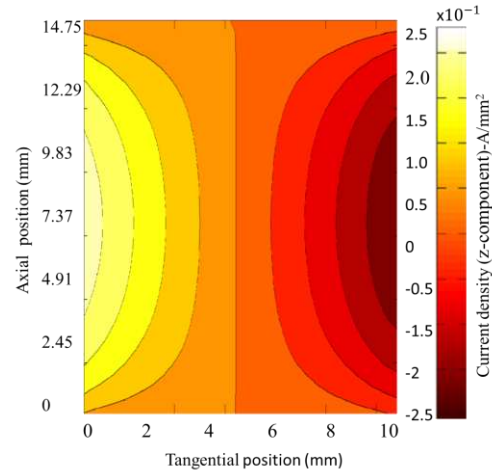


Fig.9. Eddy current density (z- component) distribution predicted by the imaging method on the outer surface of Magnet-1

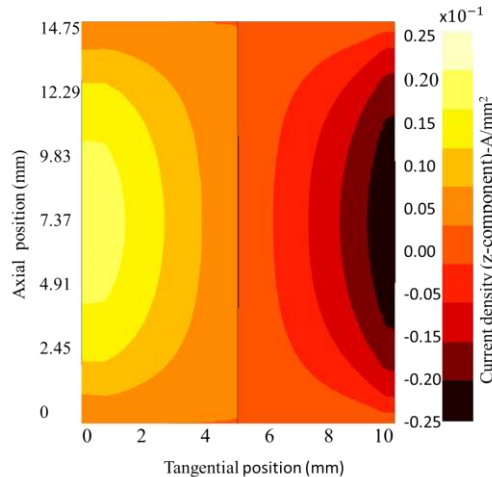


Fig.10. Eddy current density (z- component) distribution predicted by 3D FEA on the outer surface of Magnet-1

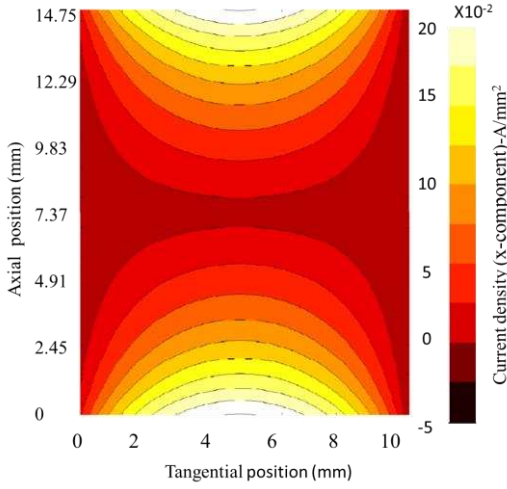


Fig.11. Eddy current density (x- component) distribution predicted by the imaging method on the outer surface of Magnet-1.

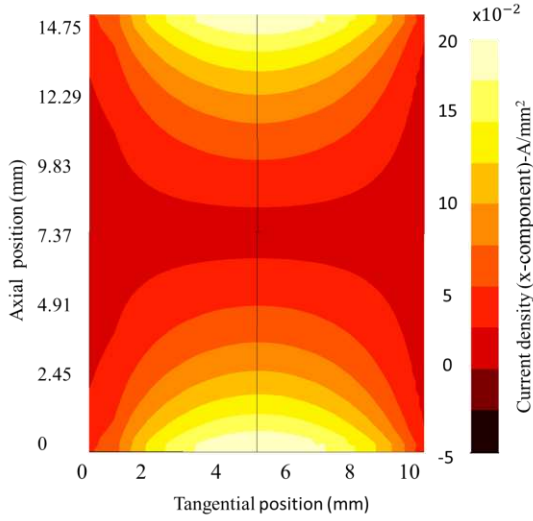


Fig.12. Eddy current density (x- component) distribution predicted by 3D FEA on the outer surface of Magnet-1.

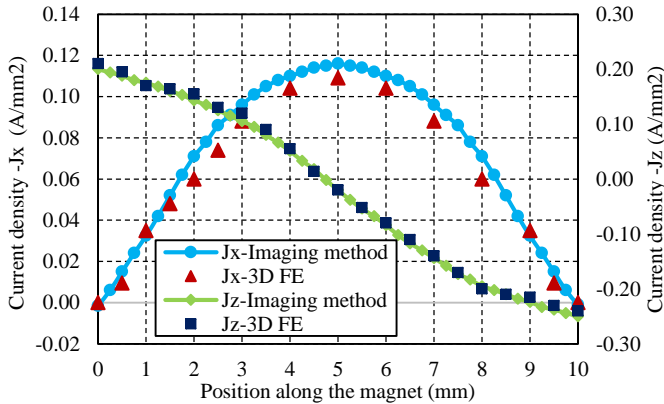


Fig.13. Variations of x and z-components of eddy current density predicted from 3D FEA and imaging method along x position at $\omega t = 12^\circ$, $y = 0.5L_y$ and $z = 0.85L_z$.

The 'z' component of eddy current density evaluated from the imaging method is compared with that obtained from 3D FEA along the middle surface of the magnet – 1 defined by

$y=1.75\text{mm}$ for the case with eight axial segments and no tangential segmentation in Fig.9 and Fig.10 at $\omega t = 12^\circ$. While Fig.11 and Fig.12 compare the 'x' component of the eddy current density evaluated from the imaging method with that obtained from 3D FEA under the same conditions. Fig.13 compares the variation of z and x components of the current density along the x- position predicted from the imaging method and 3D FEA at $z = 0.85L_z$ under previously stated conditions. It can be observed that the eddy current density distribution evaluated from the imaging method matches with the 3D FEA results. This ensures the accuracy of the proposed method.

It should be noted that the proposed method does not consider the z-component of the armature reaction fields due to the winding end effect. Detailed 3D magnetic field analysis has been performed with due account of the end-winding geometry, and the results shown that z-component of flux density close to the rotor end region is less than 5%. Since the eddy current loss in the rotor magnets is proportional to the flux density square, the resultant error is negligible.

IV. LOSS AT HIGH FREQUENCY CONSIDERING EDDY CURRENT REACTION EFFECT

To predict the magnet loss due to high frequency harmonics in the armature current where the effect of eddy current reaction becomes significant, 2D FEA results which account the reaction effect is employed in the imaging method. However, it is observed that the field variations employed in the imaging method from 2D FEA overestimates the eddy current reaction effect when the axial length of a magnet segment is relatively larger and hence the magnet loss evaluated will be lower than the actual. This is because the reaction field obtained from the 2D FEA does not account the axial variation of eddy current sources due to skin effect. Skin effect forces the eddy current to be concentrated around the magnet surfaces and its values are reduced at the center of the magnet.

To circumvent this problem a solution to the diffusion equation of the flux density along the axial ($x-z$), ($y-z$) planes are essential. The diffusion of the 'y' component of flux density $B_y(x, y_1)$ at a given ' y_1 ' along the ' $x-z$ ' plane can be expressed as,

$$\frac{\partial^2 B_y(x, y_1, z)}{\partial x^2} + \frac{\partial^2 B_y(x, y_1, z)}{\partial z^2} = j\omega\mu\sigma B_y(x, y_1, z) \quad (3)$$

Solution to (3) can be obtained considering magnet being exposed in a uniform source field of H_s and hence the field along its edges will be equal to the applied field. Since $B_s = \mu H_s$, the variation of flux density $B_y(x^1, z^1, y_1)$ for any segmentation can be evaluated in [19] as,

$$\begin{aligned} B_y(x^1, z^1, y_1) &= \frac{\cosh(\gamma x^1)}{\cosh\left(\gamma \frac{L_{xs}}{2}\right)} B_{y_1}(x^1, y_1) + \frac{8 \frac{L_{xs}}{2} \gamma^2}{\pi^2} B_{y_1}(x^1, y_1) \\ &\times \sum_{m=1}^{\infty} \frac{(-1)^m \lambda_m \cosh(\beta_m z^1)}{(2m+1)^2 \beta_m^2 \cosh\left(\beta_m \frac{L_{zs}}{2}\right)} \cos(\lambda_m x^1) \end{aligned} \quad (4)$$

where $\gamma = \frac{1+j}{\delta}$, $\lambda_m = (2m+1)\frac{\pi}{2L_{xs}}$, $\beta_m = \sqrt{\lambda_m^2 + \gamma^2}$ and δ is the skin depth.

Also $-\frac{L_{zs}}{2} \leq z^1 \leq +\frac{L_{zs}}{2}$, and $-\frac{L_{xs}}{2} \leq x^1 \leq +\frac{L_{xs}}{2}$.

A similar variation of $B_x(x^1, z^1, y_1)$ with axial position z can be derived. To assess the significance of S_x at high frequency in loss evaluation, its contribution to the magnet loss is predicted and compared with the contribution associated with S_y in Fig.14, applying the results from 2D FEA considering eddy current reaction. The loss evaluation is conducted at 20 kHz harmonics, assuming 5% amplitude of the fundamental current considered in section V when the machine operates at 4500 rpm. At these operating conditions the effect of eddy current reactions is significant. The results show that the loss associated with S_x is nearly 3 orders of magnitude lower and negligible.

Hence, $S_y(x, y, z)$ alone forms the source for eddy current loss in the permanent magnets. So $B_y(x, y)$ values obtained from 2D FEA considering reaction effect is adjusted by the ratio given in (4) at a given axial position z for the evaluation of $S_y(x, y, z)$ before application in the imaging method. hence for a given y_1 ,

$$\begin{aligned} [B_y(x, y_1, z)]_{I_M} = \\ [B_y(x, y_1)]_{2DFE} \times \frac{[B_y(x, y_1, z)]_{A_S}}{[B_y(x, y_1, z = 0.5L_z)]_{A_S}} \end{aligned} \quad (5)$$

where,

$[B_y(x, y_1, z)]_{I_M}$ are the adjusted magnetic flux density values for imaging method, $[B_y(x, y_1)]_{2DFE}$ are the flux density values from 2D FE considering reaction, $[B_y(x, y_1, z)]_{A_S}$ are the flux density values derived from (4) for any segmentation and $[B_y(x, y_1, z = 0.5L_z)]_{A_S}$ are the flux density values derived from (4) for $(-\frac{L_{xs}}{2} \leq x^1 \leq +\frac{L_{xs}}{2}$ and at $z^1 = 0$) with no axial segmentation. The maximum values of the flux density along the axial direction after adjustment is limited to values from FE without considering eddy current reaction.

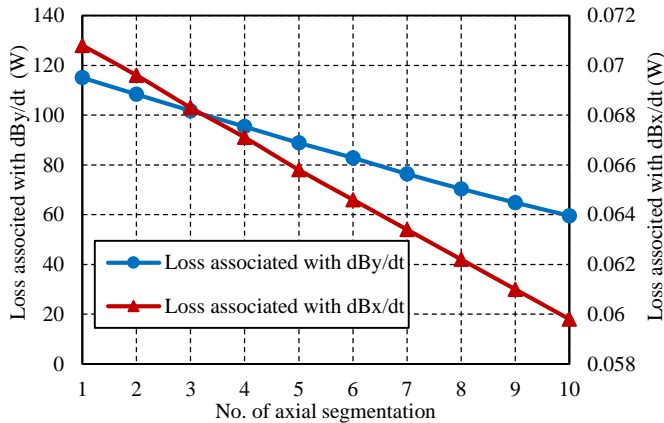


Fig.14. Comparison of loss variations associated with S_y and S_x at 20 kHz.

Since $B_y(x, y)$ evaluated from the 2D FEA includes its variation in the radial direction, the values evaluated with (5) also includes the variation along the radial direction, at the approximation of same rate as that in the x - z plane.

The predicted loss variations by the proposed method with increase in axial number of segmentations at 20 kHz are compared with 3D FEA results, and the results obtained from the imaging method based on 2D FEA source data with and without accounting eddy current reaction are compared in Fig.15 and Fig.16. The results show that the loss evaluated from the proposed method has good agreement with 3D FE results. It can be observed that there is a slight miss match especially when tangential segments=1, at lower axial segmentation numbers which can be attributed to the simplifications made in solving the diffusion equation (3) as the saturation effect of steel laminations is neglected. The difference in loss prediction with 3D FE results reduces with increase in axial segmentation as with reduction in segment width the source variation tends to become more or less uniform and go close to 2D FE source data not accounting eddy current reaction.

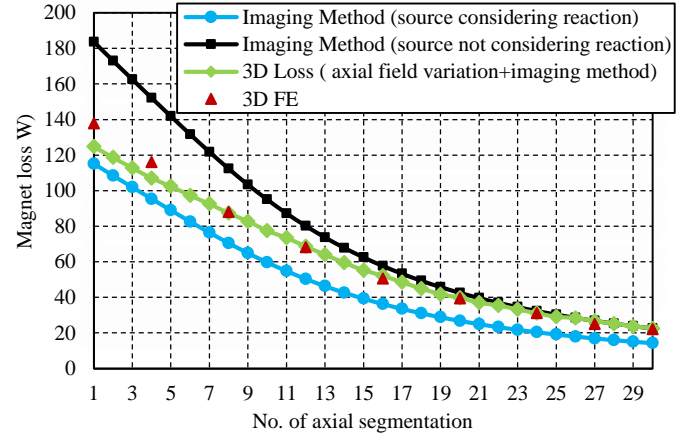


Fig.15. Comparison of loss variations with increase in axial number of segmentations, tangential segment =1 (20 kHz).

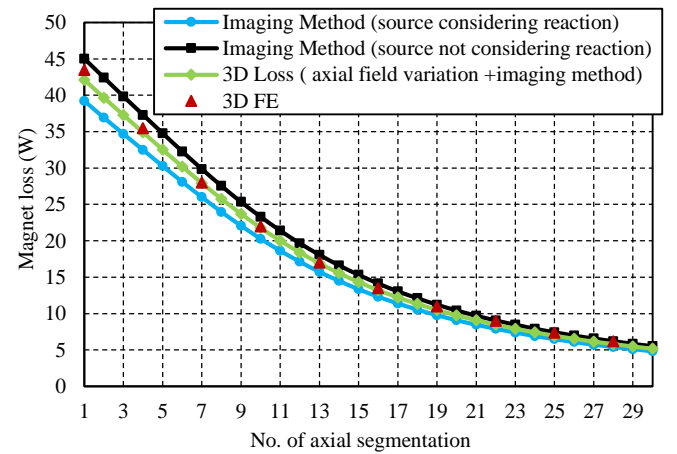


Fig.16. Comparison of loss variations with increase in axial number of segmentations, tangential segment =2 (20 kHz).

It is evident that the imaging method which employs 2D FEA results without accounting the eddy current reaction

overestimates the loss since the resistance limited eddy current distribution is no longer true. In contrast, the imaging method which employs 2D FEA results accounting the eddy current reaction underestimates the loss since the reaction field is not as strong as the 2D predictions. As the number of axial segmentations increases, the differences between the two predictions become less, and they are closer to the 3D predictions as will be expected.

V. COMBINED MAGNET LOSS EVALUATION CONSIDERING ALL ARMATURE HARMONICS.

A. Cause of Discrepancy in Total Magnet Loss and Solution by Frozen Permeability Method.

Magnet losses for an IPM machine associated with the fundamental component and high frequency pulse width modulation (PWM) harmonics are evaluated separately so far. It is intuitive to assume that the total loss can be evaluated as the sum of these individual losses associated with each harmonic. However, for the IPM machine under the operating conditions specified, it is observed that the loss evaluated from the summation of harmonic losses predicted separately is lower than the actual magnet loss which results with all the harmonics together in the supply current. This is caused by core saturation. When the high frequency harmonic current is excited separately, the core saturation level is much low, and hence the magnets buried in the rotor core are better shielded from the alternating field of the armature reaction, and the resultant loss is lower. Hence, more accurate magnet loss evaluation demands all the current harmonics to be treated together. While all the lower order harmonics for which the induced eddy current is resistance limited may be treated together, the presence of high frequency harmonics in the armature currents may result in significant eddy current reaction in magnets as explained previously and the variation of the associated eddy current sources along the axial plane for each of them need to be evaluated separately. This demands the magnet loss evaluation separately for all the higher order source harmonics influenced by skin effect.

The same dilemma exists for 3D FE prediction of eddy current loss due to a combination of low and high frequency current harmonics. In order to predict high frequency, eddy current loss accurately, the mesh size and time step have to be sufficiently small whereas the simulation time duration has to be sufficiently longer, at least one sixth of the fundamental period. Consequently, the computation time and required memory size will be enormous.

The reason for discrepancy in the total magnet loss with the summation of the harmonic loss evaluated separately arise from the highly nonlinear nature of the interior permanent magnet machines [22]. Since the machine laminations are operating mainly on the nonlinear region of the B-H curve, as shown in Fig.17, its permeability varies with the amplitude of the armature current (or field intensity H). It can be seen from Fig.17 that the sum of the fundamental excitation H_{fd} and the high frequency harmonic excitation H_{hf} will result in an increase in flux density from B_{hf} to $B_{combined}$. However the

flux density associated with combined field, $B_{combined}$ is not equal to the superposition of those associated with the fundamental and harmonic excitations. Hence, $B_{combined} < B_{fd} + B_{hf}$. Consequently, time-varying flux density experienced by the magnets is a non-linear function of the excitation current, and hence the principle of superposition is no longer valid

To circumvent this problem the frozen permeability concept [35], [36] may be employed. If the apparent relative permeability is fixed at a specific value $\mu_{combined}$, given by slope of the line 'oeda' as shown in Fig. 17, the resultant B-H relationship is a straight line with a slope of $\mu_{combined}$. Therefore, the working points under the fundamental and harmonic excitations are points "d" and "e", respectively, where the flux densities are B_{fd_FP} and B_{hf_FP} . In this case, $B_{combined} = B_{fd_FP} + B_{hf_FP}$, which implies the principle of superposition is applicable with the frozen permeability concept.

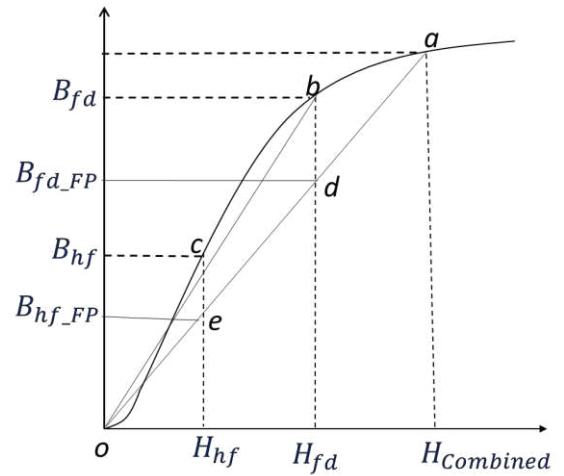


Fig.17. Illustration of the frozen permeability for magnet loss considering harmonics.

B. Method of Implementation and Validation of Results.

In order to separate the loss associated with different harmonics using the concept of frozen permeability, a sequence of dedicated processes for 1/6th electrical period as illustrated in the flow chart of Fig.18 has to be performed.

First, time-stepped 2D FEA is performed for the machine over 1/6 of an electrical cycle with all the significant low frequency current harmonics in the armature current. The size of the time-step should be sufficiently small to consider the highest frequency harmonics. At each time step or each rotor position, relative permeability of each element in the stator and rotor cores are stored as spatial quantities. Thereafter, the magnetic properties for the stator and rotor cores are updated from the original B-H curves to the spatial quantities at every time step. Subsequently, 2D FE is performed with each armature harmonic content with the stored spatial quantities at every time step to obtain the eddy current source data to be used in the 3D imaging method.

The 3D eddy current loss in the magnets of the 18-slot, 8-

pole IPM machine is evaluated by applying the frozen permeability concept when it operates at 4500rpm and is excited with the fundamental current and the high frequency switching harmonics. The dominant switching harmonics usually occur at the integer multiple of the switching frequencies ranging from a few kHz to a few tens kHz and may also have magnitudes up to a few percent of the fundamental depending on the switching frequency and the control strategy employed. 20kHz and 10kHz switching frequency harmonics with each 5% amplitude (of the fundamental) together with the fundament over 1/6th electrical cycle as shown in Fig.19 is considered in predicting the total eddy current loss. The same amplitude is selected for the loss comparison in both cases (20kHz and 10kHz) to see the effect of eddy current reaction at multiples of switching frequencies.

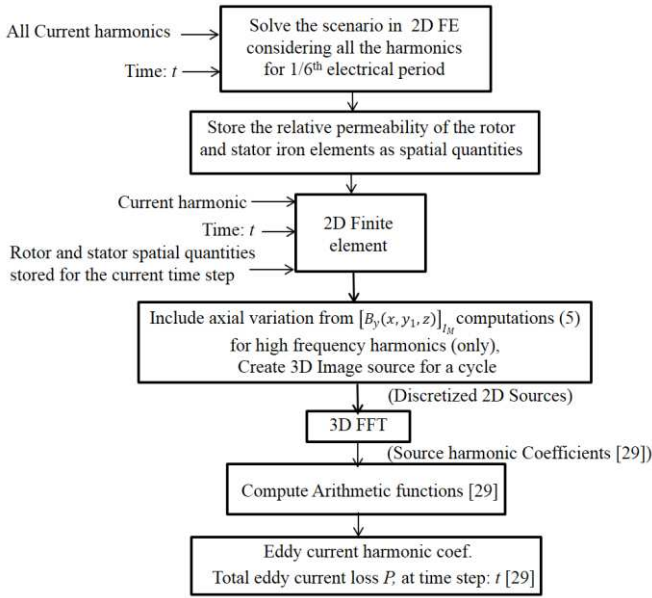


Fig.18. Flow chart showing the magnet loss evaluation at a specific harmonic employing frozen permeability.

The variations of magnet loss associated with different harmonics and the total loss evaluated are compared with 3D FEA predictions in Fig.20. It is clear from the results that the loss associated with different harmonics add together to form the total magnet loss. Further, the results from the figure shows that the loss at each harmonic evaluated by employing frozen permeability is greater than the loss evaluated at the same harmonic frequency evaluated previously in Section V and VI when magnetic saturation under a given operating condition is not appropriately accounted. This is because with the presence of the fundamental current, the saturation level in the rotor core is much high, and hence its shielding effect to high frequency field harmonics is reduced. It should also be noted that while the eddy current loss associated with the fundamental component is quite low, the losses associated with the PWM frequency harmonics are much greater even the harmonic current magnitude is only 5% of the fundamental. The losses associated with high frequency current harmonics need to be accurately evaluated and reduced in order to ensure the rotor temperature is not excessive.

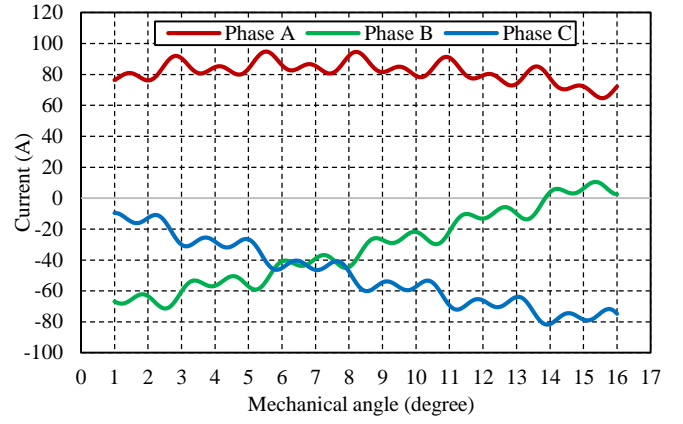


Fig.19. Armature current considering all harmonics applied for 1/6th electrical cycle.

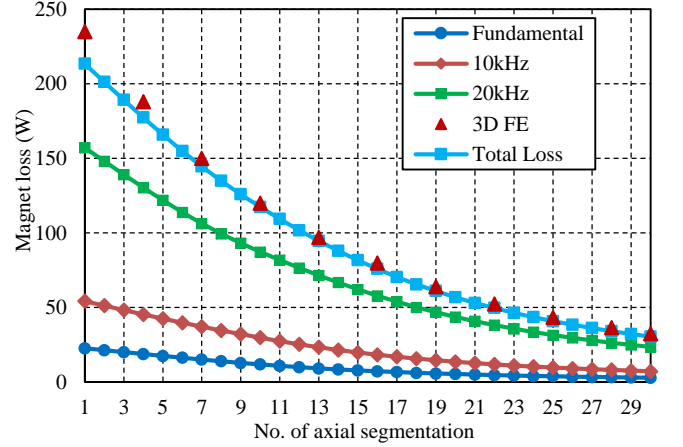


Fig.20. Variations of magnet losses with number of axial segments evaluated at different harmonics employing frozen permeability (number of tangential segment = 1).

VI. CONCLUSIONS

A method for predicting 3D eddy current loss in the rotor magnets of IPM machines has been developed based on the generalized image theory considering source variations from 2D FEA. The results obtained by accounting axial source variation in the imaging technique gave more accurate results for magnet loss at high frequencies when eddy current reaction is significant in IPM machine. The actual loss in the machine due to all the armature current harmonics is established by evaluating each harmonic loss separately by employing frozen permeability.

The results obtained show insignificance of the tangential source component in eddy current loss. For loss evaluation at each harmonic employing frozen permeability it takes around 9 hours to generate the flux density harmonics from the 2D FEA and less than 30 seconds to compute the total 3D eddy current loss for all the magnets in a typical PC. Hence on an average for evaluating the loss variation with number of axial segments up to 30, it takes around 18 minutes for each case, in contrast to more than 10 days usually required for one 3D FE analysis with no axial segmentation. The developed technique provides a computationally efficient tool for assessing the eddy current loss in the rotor magnets and for minimizing its impact on the machine performance.

REFERENCES

- [1] A. Fratta, A. Vagati, and F. Villata, "On the evolution of AC machines for spindle drive applications," *Industry Applications, IEEE Transactions on*, vol. 28, pp. 1081-1086, 1992.
- [2] H. Chen, R. Qu, J. Li, and D. Li, "Demagnetization Performance of a 7 MW Interior Permanent Magnet Wind Generator with Fractional-slot Concentrated Windings," *Magnetics, IEEE Transactions on*, vol. PP, pp. 1-1, 2015.
- [3] M. Barcaro, A. Faggion, L. Sgarbossa, N. Bianchi, and S. Bolognani, "Performance evaluation of an integrated starter alternator using an interior permanent magnet machine," *Electric Power Applications, IET*, vol. 4, pp. 539-546, 2010.
- [4] A. M. El-Refai, J. P. Alexander, S. Galioto, P. B. Reddy, H. Kum-Kang, P. de Bock, et al., "Advanced High-Power-Density Interior Permanent Magnet Motor for Traction Applications," *Industry Applications, IEEE Transactions on*, vol. 50, pp. 3235-3248, 2014.
- [5] X. Chen, J. Wang, and A. Griffo, "A High-Fidelity and Computationally Efficient Electro-thermally Coupled Model for Interior Permanent-Magnet Machines in Electric Vehicle Traction Applications," *Transportation Electrification, IEEE Transactions on*, vol. PP, pp. 1-1, 2015.
- [6] K. Urase, N. Yabu, K. Kiyota, H. Sugimoto, A. Chiba, M. Takemoto, et al., "Energy Efficiency of SR and IPM Generators for Hybrid Electric Vehicle," *Industry Applications, IEEE Transactions on*, vol. 51, pp. 2874-2883, 2015.
- [7] T. M. Jahns and R. C. Van Nocker, "High-performance EHA controls using an interior permanent magnet motor," *Aerospace and Electronic Systems, IEEE Transactions on*, vol. 26, pp. 534-542, 1990.
- [8] L. Sun-Kwon, K. Gyu-Hong, and H. Jin, "Finite Element Computation of Magnetic Vibration Sources in 100 kW Two Fractional-Slot Interior Permanent Magnet Machines for Ship," *Magnetics, IEEE Transactions on*, vol. 48, pp. 867-870, 2012.
- [9] T. M. Jahns, "Flux-Weakening Regime Operation of an Interior Permanent-Magnet Synchronous Motor Drive," *Industry Applications, IEEE Transactions on*, vol. IA-23, pp. 681-689, 1987.
- [10] S. R. Macminn and T. M. Jahns, "Control techniques for improved high-speed performance of interior PM synchronous motor drives," *Industry Applications, IEEE Transactions on*, vol. 27, pp. 997-1004, 1991.
- [11] J. Cheol, S. Ji-Yun, and H. In-Joong, "Flux-Weakening Control of IPM Motors With Significant Effect of Magnetic Saturation and Stator Resistance," *Industrial Electronics, IEEE Transactions on*, vol. 55, pp. 1330-1340, 2008.
- [12] K. Yamazaki, Y. Kanou, Y. Fukushima, S. Ohki, A. Nezu, T. Ikemi, et al., "Reduction of Magnet Eddy-Current Loss in Interior Permanent-Magnet Motors With Concentrated Windings," *Industry Applications, IEEE Transactions on*, vol. 46, pp. 2434-2441, 2010.
- [13] K. Yamazaki and K. Kitayuguchi, "Teeth shape optimization of surface and interior permanent-magnet motors with concentrated windings to reduce magnet eddy current losses," in *Electrical Machines and Systems (ICEMS), 2010 International Conference on*, 2010, pp. 990-995.
- [14] S. Chaithongsuk, N. Takorabet, and S. Kreuawan, "Reduction of Eddy-Current Losses in Fractional-Slot Concentrated-Winding Synchronous PM Motors," *Magnetics, IEEE Transactions on*, vol. 51, pp. 1-4, 2015.
- [15] J. Li, Y. Xu, and J. Zou, "Analysis and Reduction of Magnet Loss by Deepening Magnets in Interior Permanent Magnet Machines with a Pole/Slot Ratio of 2/3," *Magnetics, IEEE Transactions on*, vol. PP, pp. 1-1, 2015.
- [16] V. I. Patel, J. Wang, and S. S. Nair, "Demagnetization Assessment of Fractional-Slot and Distributed Wound 6-Phase Permanent Magnet Machines," *Magnetics, IEEE Transactions on*, vol. 51, pp. 1-11, 2015.
- [17] J. D. McFarland and T. M. Jahns, "Investigation of the Rotor Demagnetization Characteristics of Interior PM Synchronous Machines During Fault Conditions," *Industry Applications, IEEE Transactions on*, vol. 50, pp. 2768-2775, 2014.
- [18] H. Seok-Hee, T. M. Jahns, and Z. Q. Zhu, "Analysis of Rotor Core Eddy-Current Losses in Interior Permanent-Magnet Synchronous Machines," *Industry Applications, IEEE Transactions on*, vol. 46, pp. 196-205, 2010.
- [19] K. Yamazaki and Y. Fukushima, "Effect of Eddy-Current Loss Reduction by Magnet Segmentation in Synchronous Motors With Concentrated Windings," *Industry Applications, IEEE Transactions on*, vol. 47, pp. 779-788, 2011.
- [20] K. Yamazaki and A. Abe, "Loss Investigation of Interior Permanent-Magnet Motors Considering Carrier Harmonics and Magnet Eddy Currents," *Industry Applications, IEEE Transactions on*, vol. 45, pp. 659-665, 2009.
- [21] A. Bettayeb, X. Jannot, and J. C. Vannier, "Analytical calculation of rotor magnet eddy-current losses for high speed IPMSM," in *Electrical Machines (ICEM), 2010 XIX International Conference on*, 2010, pp. 1-6.
- [22] M. Paradkar and J. Bocker, "3D analytical model for estimation of eddy current losses in the magnets of IPM machine considering the reaction field of the induced eddy currents," in *Energy Conversion Congress and Exposition (ECCE), 2015 IEEE*, 2015, pp. 2862-2869.
- [23] A. Balamurali, C. Lai, A. Mollaeian, V. Loukanov, and N. Kar, "Analytical Investigation of Magnet Eddy Current Losses in Interior Permanent Magnet Motor Using Modified Winding Function Theory Accounting for Pulse Width Modulation Harmonics," *Magnetics, IEEE Transactions on*, vol. PP, pp. 1-1, 2016.
- [24] Y. Kawase, T. Ota, and H. Fukunaga, "3-D eddy current analysis in permanent magnet of interior permanent magnet motors," *Magnetics, IEEE Transactions on*, vol. 36, pp. 1863-1866, 2000.
- [25] K. Yamazaki and S. Watari, "Loss analysis of permanent-magnet motor considering carrier harmonics of PWM inverter using combination of 2-D and 3-D finite-element method," *Magnetics, IEEE Transactions on*, vol. 41, pp. 1980-1983, 2005.
- [26] K. Yamazaki and Y. Kanou, "Rotor Loss Analysis of Interior Permanent Magnet Motors Using Combination of 2-D and 3-D Finite Element Method," *Magnetics, IEEE Transactions on*, vol. 45, pp. 1772-1775, 2009.
- [27] T. Okitsu, D. Matsushashi, and K. Muramatsu, "Method for Evaluating the Eddy Current Loss of a Permanent Magnet in a PM Motor Driven by an Inverter Power Supply Using Coupled 2-D and 3-D Finite Element Analyses," *Magnetics, IEEE Transactions on*, vol. 45, pp. 4574-4577, 2009.
- [28] Z. Peng, G. Y. Sizov, H. Jiangbiao, D. M. Ionel, and N. A. O. Demerdash, "Calculation of Magnet Losses in Concentrated-Winding Permanent-Magnet Synchronous Machines Using a Computationally Efficient Finite-Element Method," *Industry Applications, IEEE Transactions on*, vol. 49, pp. 2524-2532, 2013.
- [29] L. Chen, J. Wang, and S. S. Nair, "An analytical method for predicting 3D eddy current loss in permanent magnet machines based on generalized image theory," *Magnetics, IEEE Transactions on*, vol. PP, pp. 1-1, 2015.
- [30] L. Chen, D. Hopkinson, J. Wang, A. Cockburn, M. Sparkes, and W. O'Neill, "Reduced Dysprosium permanent magnets and their applications in electric vehicle traction motors," *Magnetics, IEEE Transactions on*, vol. PP, pp. 1-1, 2015.
- [31] J. Wang, V. I. Patel, and W. Weiya, "Fractional-Slot Permanent Magnet Brushless Machines with Low Space Harmonic Contents," *Magnetics, IEEE Transactions on*, vol. 50, pp. 1-9, 2014.
- [32] P. Lazari, J. Wang, and C. Liang, "A Computationally Efficient Design Technique for Electric-Vehicle Traction Machines," *Industry Applications, IEEE Transactions on*, vol. 50, pp. 3203-3213, 2014.
- [33] L. Chen, J. Wang, P. Lombard, P. Lazari, and V. Leconte, "Design optimisation of permanent magnet assisted synchronous reluctance machines for electric vehicle applications," in *Electrical Machines (ICEM), 2012 XXth International Conference on*, 2012, pp. 2647-2653.
- [34] C. Liang, J. Wang, P. Lazari, and C. Xiao, "Optimizations of a permanent magnet machine targeting different driving cycles for electric vehicles," in *Electric Machines & Drives Conference (IEMDC), 2013 IEEE International*, 2013, pp. 855-862.
- [35] X. Chen, J. Wang, V. I. Patel, P. Lazari, L. Chen, and P. Lombard, "Reluctance torque evaluation for interior permanent magnet machines using frozen permeability," in *Power Electronics, Machines and Drives (PEMD 2014), 7th IET International Conference on*, 2014, pp. 1-6.
- [36] W. Q. Chu and Z. Q. Zhu, "Average Torque Separation in Permanent Magnet Synchronous Machines Using Frozen Permeability," *Magnetics, IEEE Transactions on*, vol. 49, pp. 1202-1210, 2013.

Sreeju S Nair (S'14) received B.Tech. degree in electrical and electronics engineering from National Institute of Technology, Calicut, in 2002, and received M.Tech. degree in electrical engineering from Indian Institute of Technology, Madras, India, in 2006, respectively. Currently he is working towards the Ph.D degree in the Dept. of Electronic and Electrical Engineering, The University of Sheffield, UK. His current research interests include eddy current loss evaluation in permanent magnet machines and partial demagnetization of permanent-magnet synchronous machines under fault conditions.

Jiabin Wang (SM'03) received the B.Eng. and M.Eng. degrees in electrical and electronic engineering from Jiangsu University of Science and Technology, Zhengjiang, China, in 1982 and 1986, respectively, and the Ph.D. degree in electrical and electronic engineering from the University of East London, London, U.K., in 1996. He is currently a Professor in electrical engineering with the University of Sheffield, Sheffield, U.K. His research interests range from motion control to electromagnetic devices and their associated drives in applications ranging from automotive and household appliances to aerospace sectors.

Liang Chen received the B.Eng. degree in 2006 and M.Eng degree in 2010, from Hefei University of Technology and Tsinghua University, China respectively. He is currently working towards the Ph.D. degree in the Department of Electronic and Electrical Engineering, The University of Sheffield, UK on design optimization of EV traction machines.

Robert Chin is currently the global research area manager at ABB corporate research, his main fields of interests are electromagnetics, thermal management, acoustics, dielectric and energy storage.

Iakovos Manolas was born in Athens, Greece, on August 3, 1983. He studied electrical and computer engineering at the National Technical University of Athens (NTUA), and received his Ph.D. in electrical engineering from the same institution in 2010. His employment experience includes research positions in the academia and research and management positions with ABB AB, Corporate Research. His special fields of interest include electrical machine design and motion control.

Dmitry Svechkarenko received his BSc degree in electromechanics from the Kyrgyz Technical University, Bishkek, Kyrgyzstan in 2002. His MSc degree and PhD degrees in electrical engineering were received from the Royal Institute of Technology, Stockholm, Sweden in 2004 and 2010, respectively. In 2010 he has joined ABB AB, Corporate Research in Västerås, Sweden where he is employed as a Senior Scientist in the field of electrical machines. His main fields of interest include electromagnetic and thermal design of electrical machines.